Research article

Fabrication of NIPMAM based polymer microgel network assisted rhodium nanoparticles for reductive degradation of toxic azo dyes

Sadia Iqbal [a], Nimra Iqbal [a], Sara Musaddiq [a,*], Zahoor Hussain Farooqi [b], Mohamed A. Habila [c], Saikh Mohammad Wabaidur [c], Amjad Iqbal [d]

[a] Department of Chemistry, The Women University Multan, 66000, Pakistan
[b] School of Chemistry, University of The Punjab, Lahore, 54590, Pakistan
[c] Chemistry Department, College of Science, King Saud University, Riyadh 11451, Saudi Arabia
[d] Faculty of Materials Engineering, Silesian University of Technology, Gliwice 44-100 , Poland

A B S T R A C T

The aim of this study was to prepare poly-N-isopropylmethacrylamide-*co*-acrylic acid-acrylamide [p-(NIPMAM-*co*-AA-AAm)] via precipitation polymerization in an aqueous medium. Rhodium nanoparticles were formed in the microgel network by an in-situ reduction technique with the addition of sodium borohydride as a reducing agent. Pure p-(NIPMAM-co-AA-AAm) and hybrid microgels [Rh-(*p*-NIPMAM-co-AA-AAm)] microgels were examined by using UV–Visible, FTIR (Fourier Transform Infrared), SEM (Scanning Electron Microscopy), TEM (Transmission Electron Microscopy), DLS (Dynamic Light Scattering) and XRD (X-Ray Diffraction) techniques. The catalytic activities of the hybrid microgel [Rh-(*p*-NIPMAM-co-AA-AAm)] for the degradation of azo dyes such as alizarin yellow (AY), congo red (CR), and methyl orange (MO) were compared and the mechanism of the catalytic action by this system was examined. Various parameters including the catalyst amount and dye concentration influenced the catalytic decomposition of azo dyes. In order to maximize the reaction conditions for the dye's quick and efficient decomposition, the reaction process was monitored by spectroscopic analysis. The rate constants for reductive degradation of azo dyes were measured under various conditions. When k_{app} values were compared for dyes, it was found that [Rh-(*p*-NIPMAM-co-AA-AAm)] hybrid microgels showed superior activity for the degradation of MO dyes compared to the reductive degradation of CR and AY.

1. Introduction

The primary source of contamination in freshwater is wastewater. Even low concentrations of many pollutants can cause harmful effects on the environment. Water quality has been linked to several critical issues facing humanity in the 21st century [1]. Excess fertilizers, pesticides, herbicides, and aromatic chemicals that flow into rivers through rainfall pose severe risks to life [2]. Inorganic compounds contain a variety of hazardous heavy metals that threaten living organisms in water [3]. Water with a BOD of 3.5 ppm is considered relatively clean. Approximately 14,000 people die daily from water pollution, largely due to untreated wastewater in developing nations [4].

---

* Corresponding author.
  E-mail address: drsara.chem@wum.edu.pk (S. Musaddiq).

Every day in industries including paper making, leather tanning, food and fiber synthetic dyes are used in huge quantities [3]. About 15–20 % of the dyes in synthetic fibers are expected to be lost in wastewater during the production or processing process [5]. Of the reactive dyes, 60 % are azo dyes and about 12 % of many synthetic dyes are estimated to be azo dyes such as methyl orange, methyl red, methylene blue and congo red. In the textile industry more than 10,000 dyes used and 280,000 tons of these dyes are removed annually worldwide [6]. However, azo dyes have significant disadvantages as they are used in large quantities every day and their improper discarding is a main problem and may influence the health of humans and animals by converting them into cancer-causing aromatic amines [3]. Azo dyes are highly hazardous dyes that are not easily decomposed due to their complex structure and synthetic properties [7].

A main drawback of previously used techniques such as coagulation and flocculation [8] is that it leads to secondary contamination due to the overuse of coagulant [3]. The catalytic reduction method by using metal nanoparticles is considered the best method for the decomposition of harmful azo dyes among all the above-mentioned methods due to its extensive surface area, strong catalytic activity, high efficiency and exceptional capacity to transport electrons [9]. The decomposition of azo dyes, in the presence of nanocatalysts, is the most excellent approach for removing azo dyes from aqueous media [10]. Metal nanoparticles (NPs) have drawn interest as high-speed conversion catalysts. However, metal nanoparticles catalysts have some disadvantages, the surface energy of the metal nanoparticles is high, and very unstable in the nanometer region consequently the metal nanoparticles rapidly aggregate together to reduce the surface area that will reduce the catalytic activity [11]. Another issue is the inability of the reaction mixture to regenerate the bare MNPs catalyst via centrifugation or ultrafiltration. However, by impregnating the MNPs on a sturdy supporting medium, these short comings can be addressed. Polysaccharides [12], micelles [13], block copolymers [14] and microgels [15] are examples of such materials that are used to stop metal nanoparticles from aggregating. Among them, microgels are easy to synthesize, adjustable even size distribution, and quick to respond to external stimuli such as pH, temperature, and ionic strength [16].

Microgels made up of NIPMAM are of particular interest since they have volume phase transition temperature (VPTT) is 46 °C higher than *p*-NIPAM i.e. 32 °C [17]. NIPMAM has a high VPTT (46 °C) and is more hydrophobic due to extra methyl group than NIPAM. Furthermore, due to their strong hydrophobicity it speeds up the rate at which reactants access the metal NPs surface, p (NIPMAM) based microgels produce fewer blocky or large sieve-sized structures than p (NIPAM) based microgels. Hence, the rate of the catalytic reaction is accelerated [18].

These hybrid microgels have been used extensively as dye reductive degradation catalysts [19]. Shah et al. employed a poly (N-isopropylacrylamide-*co*-methacrylicacid-*co*-2-hydroxyethylmethacrylate) microgel network loaded with Ag NPs to break down methylene blue, congo red and 4-nitrophenol in an aqueous solution [20]. For the catalytic reductive degradation of methyl orange (MO), Wang et al. described the utilization of nanoparticles of titanium dioxide (TiO$_2$) injected into the network of a Poly-(-N-isopropylacrylamide-*co*-acrylic acid) microgel at varied pH and temperature conditions [21]. Farooqi et al. used Ag-p-(NIPAM-co-AA) for reduction of p-NP using various amounts of acrylic acid [22].

Until now, copper, gold and silver have generally been used in nanoplasmonics research which works only in the visible or infrared range. The applications of nanoplasmonics extend into the ultraviolet (UV) spectral range. Current study has shown that Rh has a high plasmonic UV response and it is feasible to create Rh nanoparticles with a range of less than 10 nm using chemical agents [23]. The recyclability and reusability of catalysts are significant, particularly from an economic perspective. Rhodium is a costly metal thus it is essential to regain the microgels loaded with Rh nanoparticles from the reaction latterly and to employ as a catalyst for the other cycle. While the reaction was finished, the Rh-(p-(NIPMAM-co-AA-AAm) was recovered by centrifugation. The regained Rh-(p-(NIPMAM-co-AA-AAm) catalyst was employed as a catalyst under the same condition. Rhodium NPs are extra stable than Ag and Au NPs, and their surface does not oxidize easily in water. For this reason, Rhodium nanoparticles are frequently used as catalysts in aqueous media [9]. To the best of our knowledge, no studies of the catalytic degradation of azo dyes in the presence of hybrid microgels with Rh NPs based on p-(NIPMAM-co-AA-AAm) have been published in the literature.

2. Material and methods

2.1. Materials

N-isopropylmethacrylamide (NIPMAM 97 %), N, N-methylene-bis-acrylamide (BIS 99 %), Sodium Dodecyl Sulfate (SDS 97 %), Acrylic acid (AA 97 %), Acrylamide (AAm 98 %), Ammonium persulphate (APS), Sodium borohydride (SBH) were purchased from Sigma-Aldrich. Azo dyes like methyl orange alizarin yellow, congo red and Rhodium Chloride (III) (RhCl$_3$ 99 %) also purchased from Sigma-Aldrich. Microgels and hybrid microgels dialysis was done by using distilled water.

2.2. Procedure for preparation of polymer microgel and hybrid microgel

The production of p-(NIPMAM-co-AA-AAm) polymer microgels in an aqueous solution was carried out by free radical precipitation polymerization [11]. For preparation of p-(NIPMAM-co-AA-AAm) microgel, NIPMAM (85mol%) 5.08g, AAc (4mol%) 0.1 mL, 0.177g AAm (5 %) as co-monomer, 0.046g BIS (6mol%) and 0.06g sodium dodecyl sulfate were added in 250 mL three-neck round flask and stirred along 95 mL pure water with a magnetic stirrer. With continuous N$_2$ delivery, the reaction mixture was agitated and heated to 70 °C.The entire reaction was carried out in an inert environment. When the temperature was maintained at 70 °C, 5 mL of the freshly prepared 0.05 M initiator (APS) was added. After fogging, it was suspended for 6 h. The prepared p-(NIPMAM-co-AA-AAm) microgel dispersion was then cooled and dialyzed for a week using tubes madeup of molecular porous membranes each day change of distilled water at room temperature to remove initiator, surfactant and unreacted monomer. Hybrid microgels were fabricated at room

temperature by in situ reduction of metal ions in a microgel network. It has been reported in the literature that rhodium nanoparticles were prepared by reducing rhodium ions in a microgel network [9]. For hybrid microgel preparation, the 7.5 mL prepared microgel was mixed with 12.5 mL distilled water, poured into three round-bottom flask and stirred for 30 min while supplying nitrogen to remove the dissolved oxygen from the dispersion. 0.1 M sodium hydroxide was used to bring the pH of the mixture to 8.8. Then, 5 mL of rhodium chloride ($RhCl_3$) was introduced into the flask under nitrogen purge and stirred for 1 h at room temperature. The reaction mixture was then combined with 0.0035g of sodium borohydride that had been dissolved in 5 mL distilled water. This caused the liquid to turn grayish-black. This reaction was continued for another 90 min Rh-(p-NIPMAM-co-AA-AAm) hybrid microgel dispersions were dialyzed in porous membranes for 2 h to remove the unreacted chemical species.

2.3. Procedure applied for reduction of azo dyes

Firstly, solutions of azo dyes (AY, MO and CR) of various concentrations such as 0.02 mM, 0.035 mM, 0.05 mM, 0.065 mM, 0.08 mM, 0.095 mM were prepared. A sample cell of 2.5 cm long quartz was used, to which 1.7 mL of various concentrations of dye solutions were added. 0.6 mL of sodium borohydride (SBH) and 0.05 mL of [Rh-(p-(NIPMAM-co-AA-AAm)] catalyst was added to sample cell as constant factors to investigate the degradation of azi dyes. The UV–visible spectra were recorded after 2 min interval until the solution became colorless. The same experiment was repeated for 0.095 mM dye solution and 0.6 mL of SBH as constant parameters while changing the concentration of hybrid microgel. The hybrid microgel [Rh-(poly-N-isopropylmethacrylamide-*co*-Acrylic acid-Acrylamide)] catalyst was utilized with different quantities such as 0.06 mL (60 μL), 0.07 mL (70 μL), 0.08 mL (80 μL), 0.09 mL (90 μL) and 0.1 mL (100 μL).

2.4. Characterization

Different characterization techniques are used to analyze pure and hybrid microgels. Functional groups have been identified by FTIR analysis. Both p-(NIPMAM-co-AA-AAm) microgels and [Rh-(p-NIPMAM-co-AA-AAm)] hybrid microgels were dried in an oven at 70 °C and granulated into fine powder in order to obtain a FTIR spectrum at 4000-650 cm^{-1}. ALPHA (platinum ATR) FTIR spectrophotometer was used to record the FTIR spectra. Dilute dispersions of p-(NIPMAM-co-AA-AAm) microgels and Rh-(p-(NIPMAM-co-AA-AAm) were analyzed using UV–visible spectrophotometer. UV–visible spectra were recorded through HALO DB-20. The particle size and surface morphology of p-(NIPMAM-co-AA-AAm) microgels were determined by SEM analysis. JEM-2100 Transmission Electron microscope at 200 kV was used for the analysis of dilute Rh-(p-NIPMAM-co-AA-AAm) sample. The microgel size, polydispersity and responsiveness behaviors were evaluated by DLS measurement. X-ray diffraction analysis was used to assess the characteristics related to the structure.

3. Result and discussion

3.1. Mechanism involved for the preparation of p-(NIPMAM-co-AA-AAm) microgel

The p-(NIPMAM-co-AA-Am) microgels were prepared by free radical polymerization in an aqueous medium. This method is the most excellent technique for obtaining a microgel with a uniform particle size distribution. The synthesis of microgels started when the temperature reached 70 °C. This is because at high temperatures, the initiator molecules (APS) decompose into a persulfate ($S_2O_8^{2-}$), which is further decomposed into free electrons and negatively charged free sulfate radicals (SO^{4-}). The free radical sulfate (SO^{4-}) gives electrons to –C=C- in the monomer, converts it into -C-C- and initiates polymerization [24]. When the unpaired electrons on the sulfate-free radical reacted with the monomer and started the polymerization, the range of the microgel particles greater than before during the polymerization, the solution became milky white and the refractive index of the microgel particles changed forming an insoluble polymer chain [19].

The negative charge generated by the decomposition of the initiator also contributes to the coalescence between the small precursors particles and stabilizes them. The crosslinking agent (BIS) in the reaction vessel also supports the electrostatic stability and enhancing the mechanical strength of the particles. Because the cross-linking agent interacts with the particles, cross-linking occurs between the individual chains, resulting in holes of different sizes obtained. By adding a surfactant (SDS) the correct stability and monodispersity of microgel particles are achieved. When the polymerization process is completed, the reaction solution is cooled to ambient temperature to swell the microgel particles [25].

3.2. Mechanism involved for the production of [Rh-(p-nipmam-co-AA-AAm)] hybrid microgel

To prepare rhodium nanoparticles in a p-(NIPMAM-co-AA-AAm) microgel network, dilute microgel dispersions of p-(N-isopropylmethacrylamide-co-acrylamide-acrylamide) were treated with $RhCl_3$ salt. The solution of the metal salt ($RhCl_3$) functions as a precursor of rhodium nanoparticles (NPs). SBH acts as a reducing agent in the reaction mixture and is involved in the reduction of rhodium ions. When introduced into the reaction mixture, SBH is decomposed into Na^+ ions and boron hydride ions (BH_4^{-1}). Boron hydride ions (BH_4^{-1}) are attracted to Rh^{3+} ions and converted to rhodium atoms (Rh^o) because of the existence of the lone pair. The addition of sodium borohydride (SBH) turned the color of the microgel dispersion to grayish black. This indicates that rhodium ions (Rh^{3+}) were successfully reduced to rhodium atoms (Rh^o) and rhodium nanoparticles were created in the microgel network. The extensive cross-linking of polymer chains leads to the formation of rhodium nanoparticles, as microgel particles go beyond the

nanosphere. By adding NaOH before the precursor salt, it was possible to keep the pH of the microgel dispersion greater compared to the Pka value of acrylic acid (AA). The ionization of the carboxylic acid groups in acrylic acid at this pH causes the microgel particles to swell. The preparation of [Rh-(p-NIPMAM-co-AA-AAm)] microgel is shown in Fig. 1.

3.3. Characterization of p-(NIPMAM-co-AA-AAm) and Rh-(p-nipmam-co-AA-AAm) microgels

Fourier-transform infrared analysis was used on polymer microgels to identify the functional groups in the network of pure microgels and hybrid microgels and also provides information on interactions with metal nanoparticles. Pure and hybrid microgel particles are subjected to FTIR spectra in a dry state [19]. Several peaks appeared at 2968 cm^{-1} and 2972 cm^{-1}. This indicates the C–H stretching vibration of the –CH$_3$ groups of pure and hybrid microgels. The carbonyl group in the pure microgel shows a characteristic peak at 1649 cm^{-1}, while the carbonyl group in the hybrid-type microgel is shifted to 1652 cm^{-1} by the incorporation of Rh NPs into the microgel. This shift indicates a kind of interaction between Rh NPs and the resonant electrons of the carbonyl group [26]. They reported that these moderate shifts in the coupling frequency in hybrid microgels are mainly due to the metal NP's interaction with these coupling and stretching frequencies, which causes changes in hydrophobicity and hydrophilicity. The presence of a peak at the N–H bending frequency of 3282 cm^{-1} in the spectrum of p-(NIPMAM-co-AA-AAm) microgels showed a significant interaction among water and amine groups in the polymer microgels. On the other hand, in the hybrid microgel, the strong broad N–H group peak is 3359 cm^{-1}, which can identify the interaction between the amide group of the microgel and the Rh nanoparticles. For the C=C bond, the absence of a peak of 1600–1640 cm^{-1} in both the pure and hybrid microgels indicates that no unreacted monomer is left in the microgels and that the C=C double bond is converted into a C–C single bond during the polymerization procedure [18]. The clear peak at 1528 cm^{-1} reflects the N–H bending of the amide group. The distinct peak at 1528 cm^{-1} reflects N–H bending of amide group and peak at 1453 cm^{-1} shows CH$_2$ group bending vibration. The FTIR spectra of pure microgel and hybrid microgel are shown in Fig. 2 (a) and (b) respectively.

In the ultraviolet–visible spectrum (UV–visible) of the p-(NIPMAM-co-AA-AAm) microgel dispersion, no band in the wavelength range of 200–750 nm was observed. Though, the components of the p-(NIPMAM-co-AA-AAm) microgels are visible to electromagnetic radiation in the UV visibility range [11]. The surface Plasmon resonance of rhodium NPs in the microgel network was assigned to the unique peak at 220 nm [9]. Fig. 3 demonstrate the UV–visible spectra of the diluted dispersion of p-(NIPMAM-co-AA-AAm) and [Rh-(p-(NIPMAM-co-AA-AAm)] microgels.

We investigated the surface morphology of the pure microgel particles using scanning electron microscopy (SEM). A characteristic porous morphology was observed for the p-(N-isopropylmethacrylamide-co-acrylic acid-acrylamide) microgel particles. These broad, open pores allow for easy solvent exchange with the interior part of the microgel, It could be suitable as a carrier for catalytic nanoparticles [27]. SEM analysis for polymer microgel p-(NIPMAM-*co*-AA-AAm) is shown in Fig. 4(a). TEM micrograph of Rh nanoparticles incorpated in p (NIPMAM-co-AA-AAm) microgels is shown in Fig. 4(b), which shows that spherical Rh NPs were successfully loaded into the microgel particles with an average diameter of 40 nm ± 5 nm.

The pH-sensitive and temperature-sensitive behavior of microgel was investigated using DLS analysis. When the pH of the medium rises and falls with increasing temperature, the hydrodynamic radius (R$_h$) of the microgel particles slowly increases [28]. At low pH, the microgel particle is smaller; nevertheless, when pH increases, the microgel particle enlarges as seen by a rise in R$_h$. During the pH 3.9 carboxylate groups of the acrylic acid are present in a protonated form because acrylic acid pk$_a$ is 4.3. The extent of particles therefore, stay sustained in this pH. In the event of a more rise in the pH the carboxylate groups are deprotonated as a result of which repulsion forces arise among negatively charged carboxylate groups, raising the network's osmotic pressure. Carboxylate ions are more
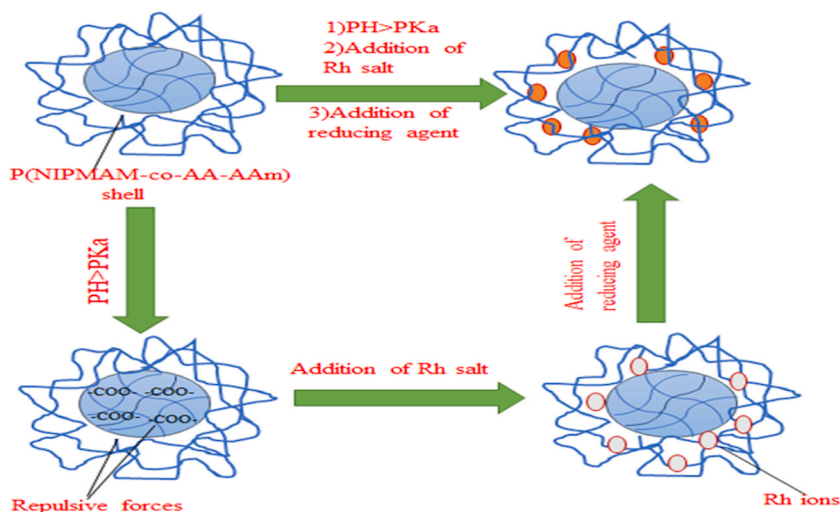

Fig. 1. Schematic demonstration for preparation of [Rh-(p-NIPMAM-co-AA-AAm)] hybrid polymer microgel.
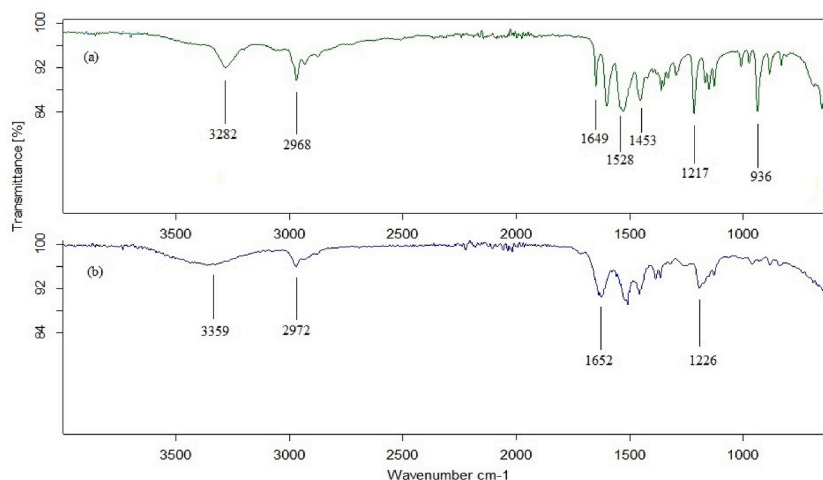
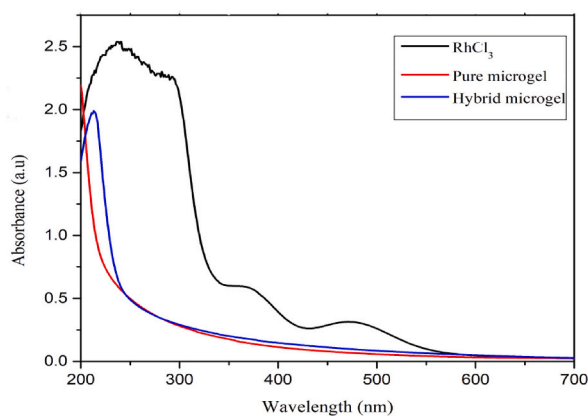**Fig. 2.** (a) FTIR spectrum of p-(NIPMAM-co-AA-AAm) (b) FTIR spectrum of [Rh-(p-(NIPMAM-co-AA-AAm)].

Fig. 3. UV–visible spectra of RhCl$_3$, p-(NIPMAM-co-AA-AAm) and [Rh-(p-(NIPMAM-co-AA-AAm)] microgel.

water loving than the carboxylic acid. More water molecules move within the microgel network and the size of the microgel increases with the rising pH of the medium. A strong increase in the hydrodynamic radius takes place in the pH range 5–7 since all carboxyl groups in this range are rapidly deprotonated. The size of the microgel particles is unaffected by a pH increase from 8 to 8.7 since all carboxyl groups are present in this pH range in protonated form. The NIPMAM component in the microgel network experiences a volume phase transition as the temperature raises, going from swollen to shrunken. The particles go through a significant phase transition as a result of water being released from the polymer matrix. The increase in the amount of H-bonds between carboxylate ions and water molecules causes the transition temperature to rise. Because of the lower degree of H-bonding and the stronger hydrophobic interaction of the polymer with water molecules only a limited number of water molecules are trapped [24]. Fig. 5 shows the hydrodynamic diameter of p-(NIPMAM-co-AA-AAm) microgel as a function of medium pH at temperature of 20 °C and 50 °C.

The different peaks in the XRD sample give information regarding the crystalline nature of the rhodium nanoparticles inside microgel network. According to published research, the main peaks for rhodium nanoparticles in this X-ray diffraction sample are 41.2°, 47°, and 69.8°, which correspond to the (111), (200), and (220) planes, respectively [29]. Lyubimov et al. notice peak at two theta values of 41.21°, which show the face-centered cubic crystal arrangement of the Rh NPs maintained by PVP polymer [30]. The average crystallite size assessed by (111) Bragg's reflection width was found to be 12 ± 5 nm. The Debye-Scherer equation was use to verify the size of crystal. XRD analysis of the [Rh-(p-N-isopropylmethacrylamide-co-acrylic acid-acrylamide)] is shown in Fig. 6.

3.4. Catalytic degradation of azo dyes

Congo red, alizarin yellow and methyl orange are chosen as substrates for this reaction since the reduction of azo dyes in the existence of nano catalysts is the most excellent approach for removing azo dyes from aqueous media. Dyes are not readily degraded by the adding up of a sodium borohydride as reducing agent since the reaction is less feasible. The electrons require to maintain a way to move rapidly from the borohydride ions (BH$_4^{-1}$) to the dye molecules. To confirm this the reduction of CR with SBH only without
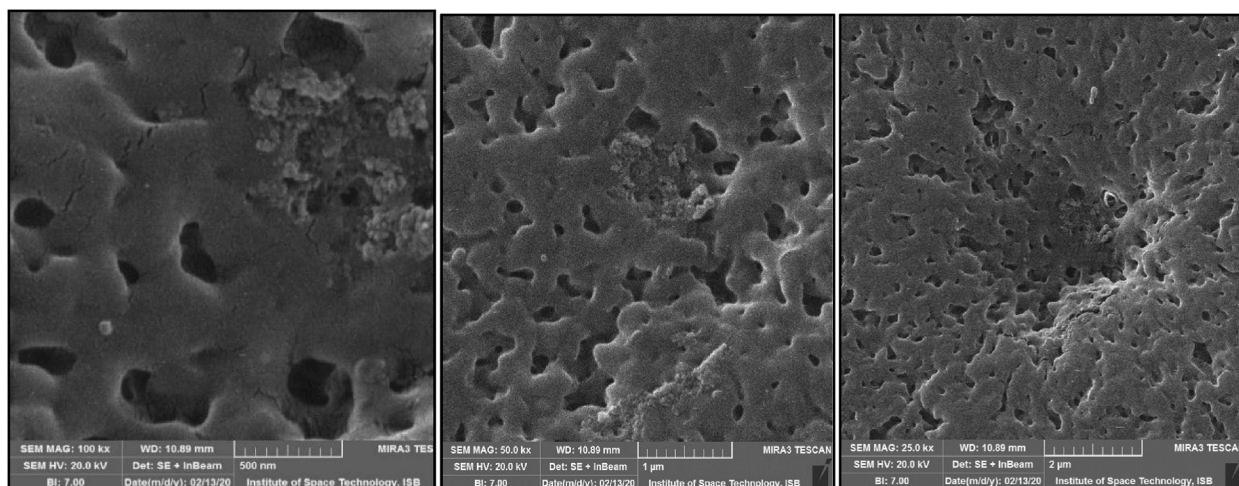
(a)
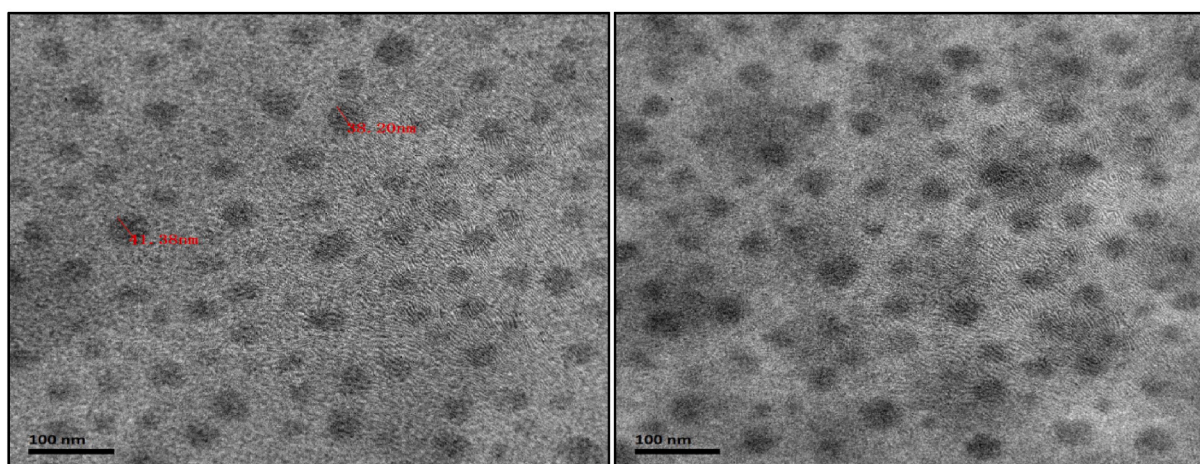
(b)

Fig. 4. (a): Scanning electron microscopy images at different focus points for p- (N-isopropylmethacrylamide-co-acrylic acid-acrylamide) microgel. **(b):** TEM images of Rh-p (N-isopropylmethacrylamide-co-acrylic acid-acrylamide) hybrid polymer microgel.
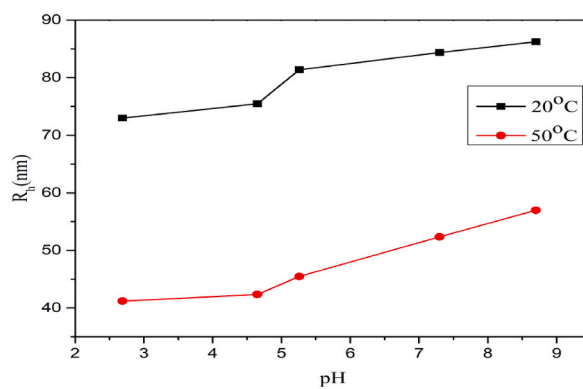

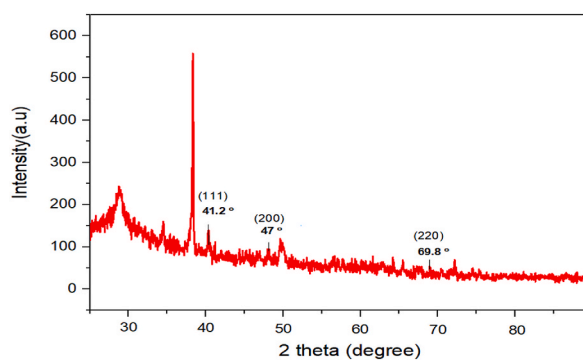**Fig. 5.** DLS analysis of p-(NIPMAM-co-AA-AAm) microgel at different temperatures.

Fig. 6. XRD analysis for [Rh-(*p*-NIPMAM-co-AA-AAm)] hybrid microgel system.

catalyst have no considerable alteration in the absorption value was found at λmax and the similar change was also observed for other dyes [9]. In Catalytic reduction of azo dyes borohydride ion (BH_4^{-1}) acts as a source of hydride ion both the dye molecule and hydride ion which are present on the surface of Rh nanoparticles. At the end of reaction product depart the metal surface and diffuse out. Degradation procedure was scanned by UV–visible spectrophotometry. The anionic dye congo red exhibits two peaks in the UV–visible range namely at 340 nm and 492 nm, which are attributable to allowed π-π* transitions and forbidden n-π*transitions. When a minute amount of catalyst was injected into the congo red (CR) solution together with sodium borohydride, a similar reduction in peak intensity could be noticed. The variation in absorption of the peak at 492 nm was investigated to check the improvement of the catalytic reduction of congo red which slowly decline over time. The n—δ* and δ—δ* transition produced two peaks at 249 and 288 nm confirming the reduction in diazo bond (-N-N-) [20]. The degradation products of congo red are biphenyl and sodium 4-amino-1-naphthalenesulfonate as shown in Fig. 7 [18]. The reduction of alizarin yellow was recorded by calculating the absorption value at 360 nm as a function of time. The decline in absorption with time because of the reduction of the azo dye by using sodium borohydride in the existence of the hybrid microgel as the catalyst. The reduction products of alizarin yellow (AY) are aniline and salicylic acid as given in Fig. 8. Methyl orange is produces a peak at 471 nm, with a second peak at 264 nm. N, N-dimethylaniline and sodium benzene sulfate are the breakdown products of methyl orange depicted in Fig. 9. The –NH$_2$ functionality of N, N-dimethylaniline show a new peak at 250 nm after decomposition [6].

The addition of a catalyst causes the dye to lose color and the intensity of the peak decreases, a clear signal that the degradation of the dye has occurred. Fig. 10(a–c) depicts the degradation pattern of various azo dyes i.e. congo red, alizarin yellow, and methyl orange. At first, characteristic peaks were observed at different wavelengths for different azo dyes which gradually decreased. In the
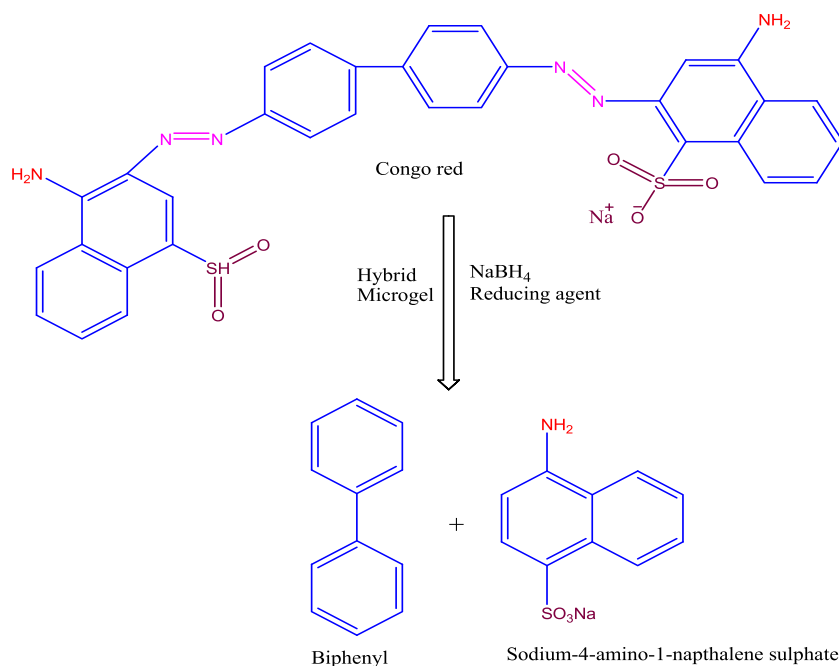

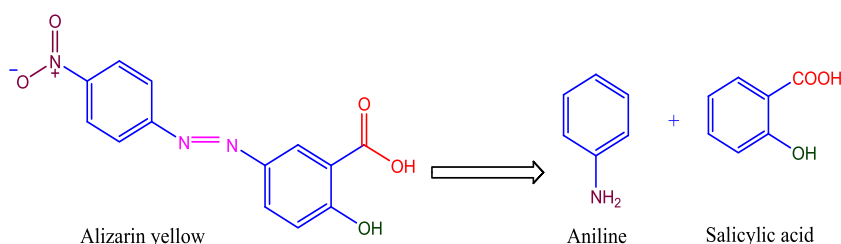**Fig. 7.** Degradation product of congo red (CR).

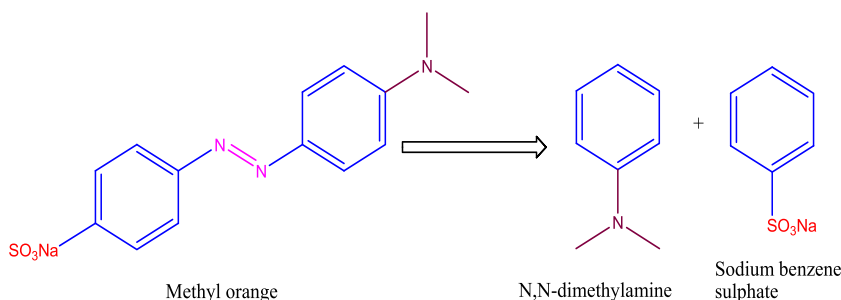**Fig. 8.** Degradation product of alizarin yellow (AY).

Fig. 9. Degradation products of methyl orange (MO).

end, a straight line was observed which indicates that no more dye content was present in the mixture. In the process of catalytic reduction of different azo dyes in the presence of hybrid catalyst, both borohydride ions and the dye molecule are directed toward the surface of Rh nanocatalyst. Borohydride ions act as a source of hydrogen and degrade the azo dyes already present on the surface of Rh nanocatalyst. As the reaction goes on, the colorful azo dye solution gradually fades and after sometime a colorless solution was observed. CR and MO azo dyes were fully degraded after 4 intervals while AY azo dye was degraded after 5 intervals as shown in Fig. 10 (a–c).

Since the amount of the catalyst is very small compared with the amount of the reducing agent (SBH) the peak intensity of the dye is not affected by the plasmon band of rhodium (Rh^0). In order to satisfy the pseudo-first-order equation, the dye concentration was kept very low in comparison with the amount of sodium borohydride (SBH). The pseudo-first-order equation is as follows.

$$ln\frac{C_t}{C_o} = ln\frac{A_t}{A_o} = -K_{app}t \tag{1}$$

In this case, A_o and A_t are the initial value and the final value of the absorption intensity of the azo dye. The degradation of azo dyes (AY, MO and CR) was carried out by varying dye concentrations and Rh-(p-NIPMAM-co-AA-AAm) catalyst concentrations. The reduction rate of each dye is changed by changing the concentration of the dye and the concentration of the hybrid microgel as a catalyst. As the dye concentration increases, the time to the end of the reaction increases and this result was obtained by applying ln (A_t/A_o) to time. The dyes concentration was varied from 0.02 mM to 0.095 mM, and hybrid microgel [Rh-(p-NIPMAM-co-AA-AAm)] and 0.6 mL sodium borohydride (SBH) were kept constant and reacted in all pigment solutions.

The time to the end of the reaction increased by the raise in the dye concentration and this result was shown in Fig. 11 (a) and (b) by applying ln (A_t/A_o) vs. time. The decrease in K_{app} values with the raise in dye concentration generally follows the Langmuir-Hinshelwood mechanism and desorption of the product from the catalyst surface to the solution takes place. By varying the amount of catalyst from 0.06 mL to 0.1 mL and the concentration of dye and SBH constant the reaction was carried out. By rising the amount of catalyst increases the number of nanoparticles (NPs) per volume thus increasing the K_{app} as given in Table 1. This was confirmed by the plot of K_{app} (min^{-1}) against the amount of catalyst, as shown in Fig. 12. A similar trend was observed for congo red and methyl orange.

3.5. Mechanism for the degradation of dye

Decomposition of sodium borohydride (SBH) produces Na^+ and BH_4^{-1} ions in the solution. The borohydride ion (BH_4^{-1}) functions as a supply source of hydride ions of both hydride ions and dye molecules present on the surface of Rh nanoparticles. When boron hydride ions (BH_4^{-1}) are present on the metal surface, hydrogen is released and electrons are transferred to Rh nanoparticles. The Rh nanoparticles acquire electrons and are activated to diazo bonds (-N=N-) of dye molecules. The conjugation weakens the diazo bond of the dye molecule and cleaves the azo bond. In the first stage of the reaction, the –N=N-is converted into a nitrogen-nitrogen single bond, which is then cleaved from the –NH–NH- bond, so that the dye becomes lighter and finally colorless. After the reaction is completed, the product leaves the metal surface and diffuses [18]. Fig. 13 shows the mechanism of catalytic decomposition of dye molecules by
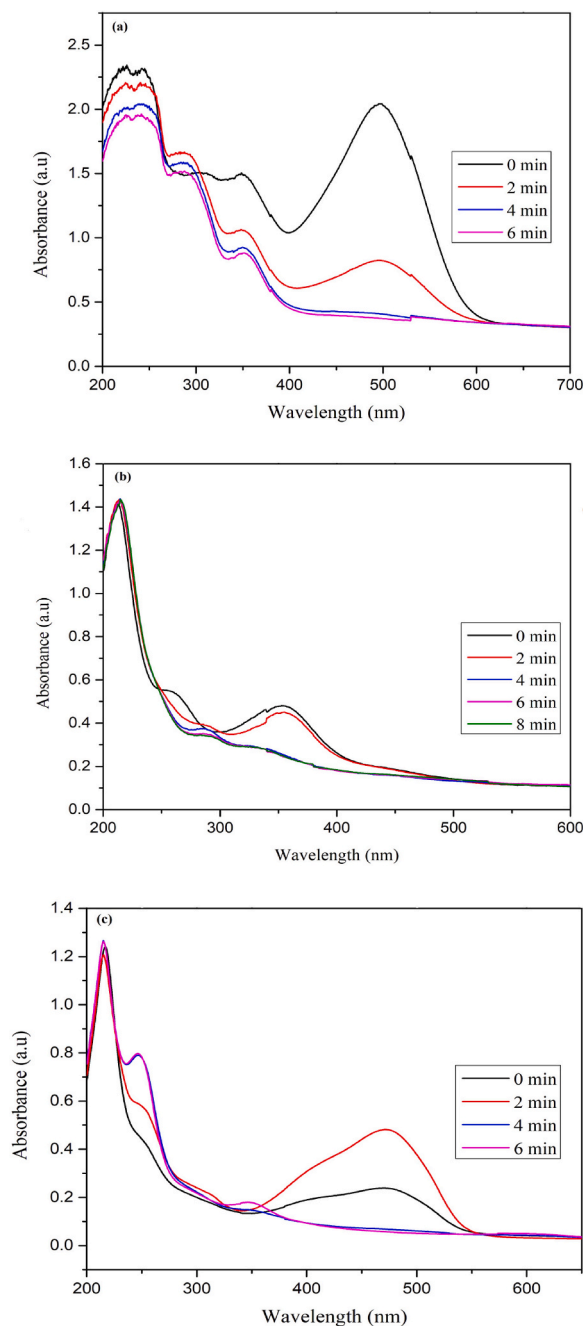
Fig. 10. Catalytic degradation of azo dyes (0.02 mM) by keeping SBH (0.6 mL) and hybrid microgel catalyst dose (0.05 μL) parameters constant at room temperature (a) Congo red degradation (b) Alizarin yellow degradation (c) Methyl orange degradation.

SBH.

4. Conclusions

Rhodium nanoparticles were successfully synthesized by means of free radical polymerization of p-(NIPMAM-*co*-AA-AAM) microgels. Rhodium nanoparticles were produced within the microgel through in-situ reduction approach by using sodium borohydride. In order to satisfy the conditions of a pseudo-first-order reaction, the hybrid microgel is used for decomposing azo dyes and converting them to less harmful components. For these reactions, rate constants observed under two different operating conditions were estimated. The K_{app} value increases initially when the dye concentration is increased while the other parameters are kept
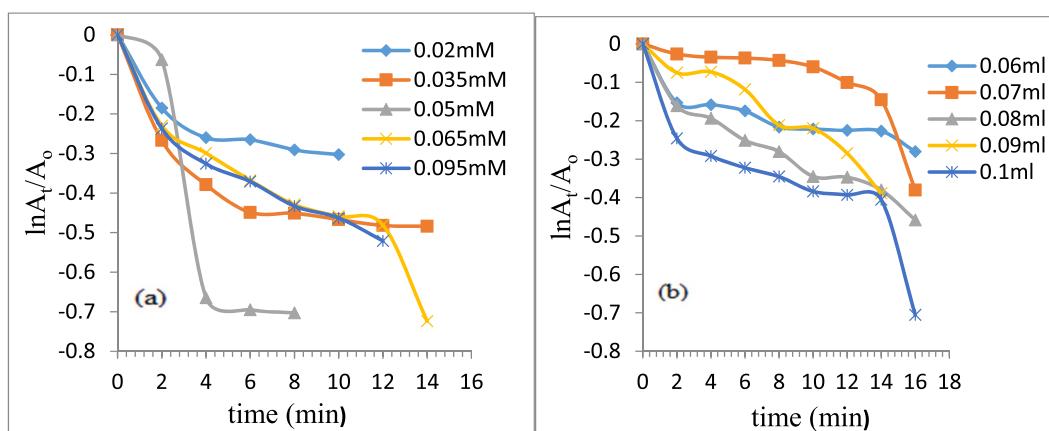
Fig. 11. The graph of ln (A_t/A_o) vs. time (a) for alizarine yellow dye reduction using various concentrations at constant catalyst doses with SBH (b) for alizarine yellow dye reduction with SBH using various Rh-(p-NIPMAM-co-AA-AAm) catalyst doses.

Table 1
Half-life and observe rate constant (K_{app}) of azo dyes for both reaction conditions.

Azo Dyes	Constant parameter	Variable parameter		K_{app} (min^{-1})	Half-life (min)
AY	Catalyst dose (50ml/0.05 µL) + SBH (0.6 mL)	Alizarine yellow concentration	0.02 mM	0.026	26.653
			0.035 mM	0.028	24.75
			0.05 mM	0.101	6.861
			0.065 mM	0.040	17.325
			0.095 mM	0.037	18.729
	Dye concentration (0.095 mM) + SBH (0.6 mL)	Catalyst dose	0.06 mL	0.012	57.75
			0.07 mL	0.017	40.764
			0.08 mL	0.024	28.875
			0.09 mL	0.025	27.72
			0.1 mL	0.029	23.896
CR	Catalyst dose (50ml/0.05 µL) + SBH (0.6 mL)	Congo red concentration	0.02 mM	0.114	6.078
			0.035 mM	0.194	3.572
			0.05 mM	0.221	3.135
			0.065 mM	0.271	2.557
			0.08 mM	0.266	2.605
			0.095 mM	0.260	2.665
	Dye concentration (0.095 mM) + SBH (0.6 mL)	Catalyst dose	0.06 mL	0.199	3.482
			0.07 mL	0.278	2.492
			0.08 mL	0.290	2.389
			0.09 mL	0.296	2.341
			0.1 mL	0.342	2.026
MO	Catalyst dose (50ml/0.05 µL) + SBH (0.6 mL)	Methyl orange Concentration	0.02 mM	0.292	2.373
			0.035 mM	0.305	2.272
			0.05 mM	0.487	1.422
			0.065 mM	0.455	1.523
			0.08 mM	0.320	2.165
	Dye concentration (0.095 mM) + SBH (0.6 mL)	Catalyst dose	0.06 mL	0.441	1.571
			0.08 mL	0.459	1.509
			0.09 mL	0.493	1.405
			0.1 mL	0.533	1.300

constant. The decline of K_{app} value by the raise of dye concentration is often related to the Langmuir-Hinshelwood mechanism in which products desorption from the catalyst surface to the solution. When the amount of the catalyst is increased, the k_{app} value is increased, it was proven that the value of k_{app} was highest when a large amount of catalyst was used. The value of the rate constant was larger in the case of MO dye however, the hybrid system also effective for the degradation of other azo dyes. Our method has the potential to convert these pollutants into less toxic molecules that can be used to produce a variety of useful compounds.

Data availability statement
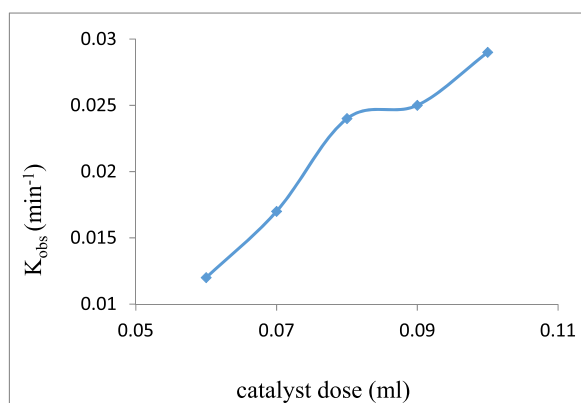
Data included in article/referenced in article.

Fig. 12. Plot of K_{app} (min^{-1}) and catalyst dose (mL) for AY.
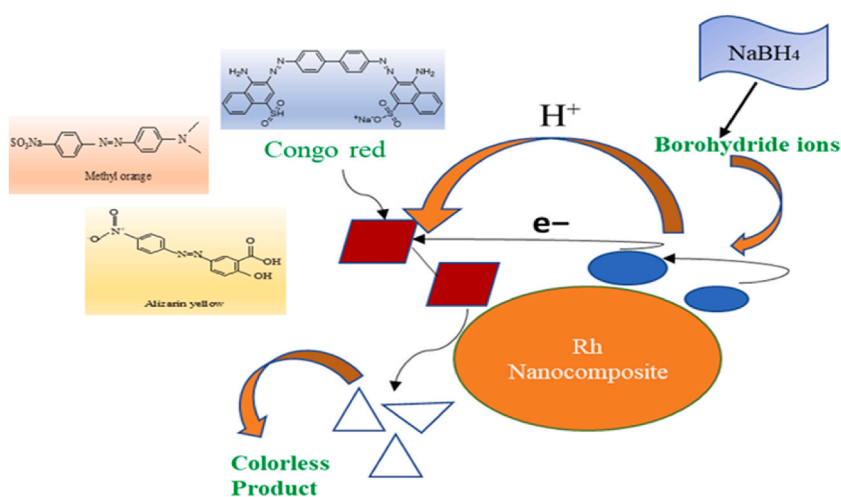

Fig. 13. Mechanism for Adsorption of reducing agent and dyes on the surface of metal nanoparticles.

Additional information

No additional information is available for this paper.

CRediT authorship contribution statement

Sadia Iqbal: Investigation, Conceptualization. **Nimra Iqbal:** Writing – original draft, Methodology, Investigation. **Sara Musaddiq:** Writing – review & editing, Validation, Supervision, Data curation, Conceptualization. **Zahoor Hussain Farooqi:** Supervision, Conceptualization. **Mohamed A. Habila:** Visualization, Project administration, Funding acquisition. **Saikh Mohammad Wabaidur:** Writing – review & editing, Visualization, Funding acquisition. **Amjad Iqbal:** Writing – review & editing, Project administration, Formal analysis, Dr.

Declaration of competing interest

The authors declare that they have no known competing financial interests or personal relationships that could have appeared to influence the work reported in this paper.

Acknowledgement

References

[1] R.P. Schwarzenbach, T. Egli, T.B. Hofstetter, U.V. Gunten, B. Wehrli, Global water pollution and human health, Annu. Rev. Environ. Resour. 35 (2010) 109–136.

[2] F. Owa, Water pollution: sources, effects, control and management, Mediterr. J. Soc. Sci. 4 (8) (2013) 1–8.

[3] D. Parasuraman, E. Leung, M.J. Serpe, Poly (N-isopropylacrylamide) microgel based assemblies for organic dye removal from water: microgel diameter effects, Colloid Polym. Sci. 290 (11) (2012) 1053–1064.

[4] L. Jiang, P. Liu, S. Zhao, Magnetic ATP/FA/Poly (AA-co-AM) ternary nanocomposite microgel as selective adsorbent for removal of heavy metals from wastewater, Colloids Surf., A 470 (2015) 31–38.

[5] D. Chatterjee, V.R. Patnam, A. Sikdar, P. Joshi, R. Misra, N.N. Rao, Kinetics of the decoloration of reactive dyes over visible light-irradiated TiO2 semiconductor photocatalyst, J. Hazard Mater. 156 (2008) 435–441.

[6] M.F. Hanafi, N. Sapawe, A review on the water problem associate with organic pollutants derived from phenol, methyl orange, and remazol brilliant blue dyes, Mater. Today: Proc. 31 (2020) A141–A150.

[7] N.P. Tantak, S. Chaudhari, Degradation of azo dyes by sequential Fenton's oxidation and aerobic biological treatment, J. Hazard Mater. 136 (3) (2006) 698–705.

[8] J. Bratby, Coagulation and Flocculation in Water and Wastewater Treatment, IWA publishing, 2016.

[9] S. Iqbal, S. Musaddiq, R. Begum, A. Irfan, Z. Ahmad, M. Azam, J. Nisar, Z.H. Farooqi, Recyclable polymer microgel stabilized rhodium nanoparticles for reductive degradation of para-nitrophenol, Z Phys Chem 235 (12) (2021) 1701–1719.

[10] L.D. Ardila-Leal, R.A. Poutou-Piñales, A.M. Pedroza-Rodríguez, B.E. Quevedo-Hidalgo, A brief history of colour, the environmental impact of synthetic dyes and removal by using laccases, Molecules 26 (13) (2021) 3813.

[11] R. Begum, K. Naseem, E. Ahmed, A. Sharif, Z.H. Farooqi, Simultaneous catalytic reduction of nitroarenes using silver nanoparticles fabricated in poly (N-isopropylacrylamide-acrylic acid-acrylamide) microgels, Colloids Surf., A 511 (2016) 17–26.

[12] M. Nasrollahzadeh, N. Shafiei, Z. Nezafat, N.S.S. Bidgoli, F. Soleimani, Recent progresses in the application of cellulose, starch, alginate, gum, pectin, chitin and chitosan based (nano) catalysts in sustainable and selective oxidation reactions: a review, Carbohydr. Polym. 241 (2020) 116353.

[13] U.T. Duong, A.B. Gade, S. Plummer, F. Gallou, S. Handa, Reactivity of carbenes in aqueous nanomicelles containing palladium nanoparticles, ACS Catal. 9 (12) (2019) 10963–10970.

[14] A.K. Taylor, D.S. Perez, X. Zhang, B.K. Pilapil, M.H. Engelhard, B.D. Gates, D.A. Rider, Block copolymer templated synthesis of PtIr bimetallic nanocatalysts for the formic acid oxidation reaction, J. Mater. Chem. A 5 (40) (2017) 21514–21527.

[15] S. Iqbal, C. Zahoor, S. Musaddiq, M. Hussain, R. Begum, A. Irfan, M. Azam, Z.H. Farooqi, Silver nanoparticles stabilized in polymer hydrogels for catalytic degradation of azo dyes, Ecotoxicol. Environ. Saf. 202 (2020) 110924.

[16] A. Alshammari, V.N. Kalevaru, Supported gold nanoparticles as promising catalysts, Catal. Appl. Nano-Gold Catal. (2016) 57–81.

[17] G. Aguirre, E. Villar-Alvarez, A. González, J. Ramos, P. Taboada, J. Forcada, Biocompatible stimuli-responsive nanogels for controlled antitumor drug delivery, J. Polym. Sci., Part A: Polym. Chem. 54 (12) (2016) 1694–1705.

[18] K. Naseem, Z.H. Farooqi, R. Begum, W. Wu, A. Irfan, A.G. Al-Sehemi, Silver nanoparticles engineered polystyrene-poly (n-isopropylmethacrylamide-acrylic acid) core shell hybrid polymer microgels for catalytic reduction of Congo red, Macromol. Chem. Phys. 219 (18) (2018) 1800211.

[19] M. Shahid, Z.H. Farooqi, R. Begum, K. Naseem, M. Ajmal, A. Irfan, Designed synthesis of silver nanoparticles in responsive polymeric system for their thermally tailored catalytic activity towards hydrogenation reaction, Kor. J. Chem. Eng. 35 (5) (2018) 1099–1107.

[20] L.A. Shah, A. Haleem, M. Sayed, M. Siddiq, Synthesis of sensitive hybrid polymer microgels for catalytic reduction of organic pollutants, J. Environ. Chem. Eng. 4 (3) (2016) 3492–3497.

[21] S.Q. Wang, Q.L. Liu, A.M. Zhu, Preparation of multisensitive poly (N-isopropylacrylamide-co-acrylic acid)/TiO2 composites for degradation of methyl orange, Eur. Polym. J. 47 (5) (2011) 1168–1175.

[22] Z.H. Farooqi, A. Ijaz, R. Begum, K. Naseem, M. Usman, M. Ajmal, U. Saeed, Synthesis and characterization of inorganic–organic polymer microgels for catalytic reduction of 4-nitroaniline in aqueous medium, Polym. Compos. 39 (3) (2018) 645–653.

[23] A.M. Watson, X. Zhang, R. Alcaraz de La Osa, J.M. Sanz, F. González, F. Moreno, G. Finkelstein, J. Liu, H.O. Everitt, Rhodium nanoparticles for ultraviolet plasmonics, Nano Lett. 15 (2) (2015) 1095–1100.

[24] M. Ajmal, Z.H. Farooqi, M. Siddiq, Silver nanoparticles containing hybrid polymer microgels with tunable surface plasmon resonance and catalytic activity, Kor. J. Chem. Eng. 30 (11) (2013) 2030–2036.

[25] S. Ashraf, R. Begum, R. Rehan, W. Wu, Z.H. Farooqi, Synthesis and characterization of pH-responsive organic–inorganic hybrid material with excellent catalytic activity, J. Inorg. Organomet. Polym. Mater. 28 (5) (2018) 1872–1884.

[26] R. Begum, Z.H. Farooqi, Z. Butt, Q. Wu, W. Wu, A. Irfan, Engineering of responsive polymer based nano-reactors for facile mass transport and enhanced catalytic degradation of 4-nitrophenol, J. Environ. Sci. 72 (2018) 43–52.

[27] T. Kamal, M.S.J. Khan, S.B. Khan, A.M. Asiri, M.T.S. Chani, M.W. Ullah, Silver nanoparticles embedded in gelatin biopolymer hydrogel as catalyst for reductive degradation of pollutants, J. Polym. Environ. 28 (2) (2020) 399–410.

[28] G. Singhal, R. Bhavesh, K. Kasariya, A.R. Sharma, R.P. Singh, Biosynthesis of silver nanoparticles using Ocimum sanctum (Tulsi) leaf extract and screening its antimicrobial activity, J. Nano Res. 13 (7) (2011) 2981–2988.

[29] N. Zettsu, J.M. McLellan, B. Wiley, Y. Yin, Z.Y. Li, Y. Xia, Synthesis, stability, and surface plasmonic properties of rhodium multipods, and their use as substrates for surface-enhanced Raman scattering, Angew. Chem. 118 (8) (2006) 1310–1314.

[30] S.E. Lyubimov, E.A. Rastorguev, K.I. Lubentsova, A.A. Korlyukov, V.A. Davankov, Rhodium-containing hypercross-linked polystyrene as a heterogeneous catalyst for the hydroformylation of olefins in supercritical carbon dioxide, Tetrahedron Lett. 54 (9) (2013) 1116–1119.